DNS and LES of separated flows at moderate Reynolds numbers

By F. Cadieux†, J. A. Domaradzki†, T. Sayadi, S. Bose AND F. Duchaine¶

Flows over airfoils and blades in rotating machinery, for unmanned and micro-aerial vehicles, wind turbines, and propellers consist of different flow regimes. A laminar boundary layer near the leading edge is often followed by a laminar separation bubble with a shear layer on top of it that experiences transition to turbulence. The separated turbulent flow then reattaches and evolves downstream from a non-equilibrium turbulent boundary layer to an equilibrium one. Typical Reynolds-averaged Navier-Stokes (RANS) turbulence modeling methods were shown to be inadequate for such separated flows by Spalart & Strelets (2000). Direct numerical simulation (DNS) is the most reliable but is also the most computationally expensive alternative. This work assesses the capability of LES to reduce the resolution requirements for such flows. Flow over a flat plate with suitable velocity boundary conditions away from the plate to produce a separation bubble is considered. Benchmark DNS data for this configuration are generated with the resolution of 59×10^6 mesh points; also used is a different DNS database with 15×10^6 points reported by Spalart & Strelets (2000). By employing two different codes, one using structured and another unstructured mesh, results confirm that accurate LES are possible using O(1%) of the DNS resolution.

1. Introduction

Reynolds numbers for flows in rotating machinery, for unmanned aerial vehicles (UAV), micro-air vehicles (MAV), wind turbines, and propellers are low to moderate. Based on wing/blade chord, they are typically less than 2×10^6 and are often only on the order of 10^4 to 10^5. By comparison, civilian airplanes are characterized by Reynolds numbers ranging from a few million to 80×10^6 for the Boeing 747 at cruising velocity. Recent experimental investigations of low Reynolds number aerodynamics (Hu *et al.* 2007; Hain *et al.* 2009; Spedding & McArthur 2010) reveal that low to moderate Reynolds number flows over airfoils and turbine blades are often dominated by the effects of flow separation. Separation greatly influences the aerodynamic forces the airfoil or blade is subjected to. Separation changes the lift and drag characteristics and thus the flight stability of UAVs. Wind turbine efficiency can be severely affected by separation. It also causes unsteadiness in turbine flows, which is a determining factor in high cycle fatigue (HCF) of turbo-machinery components.

The physical origin of laminar and transitional flow separation is qualitatively well understood: the attached laminar boundary layer developing on a wing or blade is subjected to an adverse pressure gradient due to the airfoil's curvature, which causes it to separate. Immediately behind the separation point there is an effectively stagnant flow region, the so-called dead air region, followed by a reverse flow vortex. The interface between the

† Department of Aerospace and Mechanical Engineering, University of Southern California
¶ CFD and Globc Team, Centre Européen de Recherche et de Formation Avancée en Calcul Scientifique (CERFACS)

separated flow moving away from the wing and the recirculating flow in the vicinity of the wing results in a shear layer with an inflectional mean velocity profile. This shear layer experiences Kelvin-Helmholtz instabilities that develop into turbulence after first generating characteristic spanwise vortices. Further downstream, the separated turbulent flow reattaches and gradually evolves into the classical turbulent boundary layer. The separation bubble's shape and size changes in time due to vortex shedding, making the problem inherently unsteady. The above picture emerges from numerous experimental investigations, e.g. Marxen *et al.* (2003); Hu *et al.* (2007); Hain *et al.* (2009) and Spedding & McArthur (2010), as well as from direct numerical simulations (DNS) results by Lin & L.Pauley (1996); Spalart & Strelets (2000); Alam & Sandham (2000); Marxen & Rist (2010); Jones *et al.* (2008) and Jones *et al.* (2010).

1.1. *Motivation*

In order to produce more efficient airfoil or blade designs, to create control schemes to reduce separation effects, and to better predict HCF, numerical prediction tools for laminar separation bubble flows are needed. However, computationally affordable and reliable numerical results for such flows are difficult to obtain. Typical RANS turbulence models face difficulties for separated flows because they were designed for fully developed turbulent flows. As described above, low to moderate Reynolds number flows over blades and airfoils consist of a mixture of regions where the flow is laminar, transitional, and then evolves from a non-equilibrium turbulent boundary layer to an equilibrium one. The importance of the Reynolds stresses varies widely across and even within these regions. Such variations are not accounted for in classical turbulence models. Low to moderate Reynolds number separation driven by an adverse pressure gradient as opposed to geometry is also an intrinsically non-equilibrium process. It involves subtle interactions between viscous, advective, and pressure effects that can only be reliably captured by solving the full Navier-Stokes equations, i.e. using direct numerical simulations (DNS).

However, DNS require substantial computational resources, long wall-clock runs, and long analysis time; e.g. Jones *et al.* (2008) used over 170 million grid points for a relatively simple 3-D configuration. A number of 3-D configurations and angles of attack need to be quickly investigated to allow for the optimization of airfoil and turbine blade designs. In this case, a DNS approach is not feasible and other simulation options must be considered. One option is to employ Reynolds averaged Navier-Stokes (RANS) models, modified to account for the reduction of the eddy viscosity around the separation region. This is an approach commonly used and optimized for high Reynolds number turbulent flows, but one that was tested and shown to be inadequate for the separated flows of interest by Spalart & Strelets (2000). Another option is to employ large eddy simulation (LES) techniques. For instance, Yang & Voke (2001) reported LES results obtained with the dynamic Smagorinsky in good agreement with experiments for boundary-layer separation and transition caused by surface curvature at $Re = 3,450$. Yet even for this relatively low Reynolds number, the critical issues in getting agreement was a numerical resolution ($472 \times 72 \times 64$ mesh points) comparable to DNS of the same flow and a high order numerical method. Such strict requirements are difficult to satisfy in simulations of practical flows often performed with low order finite difference or finite volume methods (e.g. commercial codes). Similarly, Eisenbach & Friedrich (2008) performed LES of flow separation on an airfoil at a high angle of attack at $Re = 10^5$ using Cartesian grids. This case also required very high resolutions between 50 and 100 million mesh points. Using LES with such high resolution and higher order methods implies a time-to-solution on the same order as DNS. Therefore, the question remains: can LES produce sufficiently

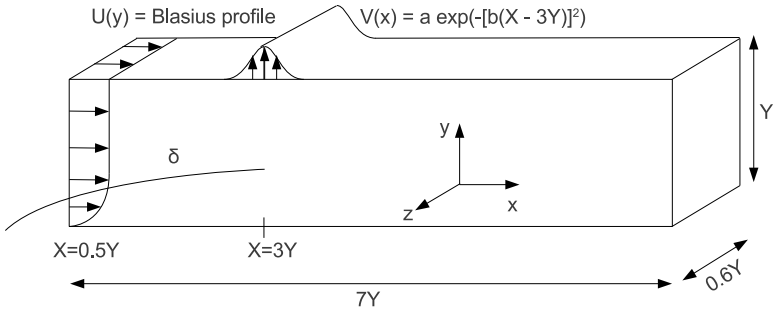

FIGURE 1. Computational domain, boundary and inlet conditions used to investigate laminar separation bubble flow

accurate results for laminar separation bubble flows with drastically reduced resolution, around 1% of DNS resolution, commonly achievable for fully turbulent flows?

2. Method

2.1. *Flow specification*

A procedure used successfully by other investigators (Wilson & Pauley 1998; Alam & Sandham 2000; Spalart & Strelets 2000) to induce separation in a flow over a flat plate is followed. The computational domain is a rectangular box with a rigid lower wall on which the boundary layer flow evolves (see Figure 1). The domain height Y is used to non-dimensionalize all relevant lengths. A laminar Blasius boundary layer velocity profile with the free stream velocity U_0 is imposed at the inflow. At the top boundary, a vertical suction velocity is imposed in a narrow slot oriented perpendicular to the mean flow direction. The suction produces an adverse pressure gradient that causes flow separation. The flow then transitions to turbulence and reattaches.

Following Spalart & Strelets (2000) the vertical suction velocity is specified as

$$V(x) = a \exp(-[(x - X_s)/(0.24Y)]^2), \tag{2.1}$$

where a is the peak velocity and X_s is its streamwise location. The resulting separation bubble is sensitive only to the upper-wall boundary conditions through the nominal flow deceleration parameter S,

$$S = \frac{1}{YU_0} \int V(x) dx. \tag{2.2}$$

Spalart & Strelets (2000) choose $X_s = 3Y$ and set $S = 0.3$ and the Reynolds number at X_s to $R_X = 10^5$, giving $a \approx 0.7U_0$ and $Re_Y = Re_X/3$. These choices are driven by the requirement that the flow separates naturally, without additional forcing mechanisms.

2.2. *Numerical methods*

In CTR simulations, the full compressible LES equations are solved for a perfect gas using sixth-order compact finite differences (Nagarajan *et al.* 2007). An implicit-explicit time integration scheme is applied. For explicit time advancement, a third-order Runge-Kutta scheme (RK3) is employed and a second-order A-stable scheme is used for the implicit portion. Compact filtering as described by Lele (1992) is employed at each time step,

both in the freestream and wall-normal directions to ensure overall stability and zonal matching at the interface between the implicit and explicit grids (Nagarajan 2004). The numerical scheme is constructed on a structured curvilinear grid, and the variables are staggered in space. The freestream Mach number is chosen to be 0.2.

Numerical sponges (Mani 2012) are used at all boundaries except at the rigid bottom wall to ensure sound and vortical waves are not reflected back into the computational domain. The inlet sponge spans from $x = 0.03Y$ to $x = 0.5Y$, whereas the outlet sponge starts at $x = 8Y$ and ends at $x = 9.2Y$. The flow is recycled from outlet to inlet by forcing a return to the desired inlet boundary layer profile. The top sponge extends the domain from $Y = 1$ to $Y = 1.8$. Sponge regions account for one third of the total number of mesh points. These sponge layers relax the computed Navier-Stokes solution to the scale-similar compressible boundary layer case obtained a priori as a reference solution. From $Y = 1$ to $Y = 1.4$, the reference solution's wall-normal velocity is forced to the suction profile specified in eq. (2.1). It is then smoothly brought back to its precomputed scale-similar value from $Y = 1.4$ to $Y = 1.8$. The sponge relaxation parameter increases from zero at $Y = 1$, the end of the physical domain, and reaches its maximum close to $Y = 1.8$. The suction velocity is thus enforced indirectly through the influence of the forced solution above the top of the physical domain. The spanwise direction is treated as periodic.

The parallel LES code AVBP (Schønfeld & Rudgyard 1999; Mendez & Nicoud 2008) solves the full compressible Navier-Stokes equations using a two-step time-explicit Taylor-Galerkin scheme (TTG4A) for the hyperbolic terms on a cell-vertex formulation (Colin & Rudgyard 2000), along with a second-order Galerkin scheme for diffusion. TTG4A provides high spectral resolution and both low numerical dissipation and dispersion, which is particularly well-suited for LES (Colin & Rudgyard 2000). Such numerics were designed specifically for LES on hybrid meshes and have been extensively validated in the context of turbulent reacting flow applications (Boileau *et al.* 2008; Staffelbach *et al.* 2009; Gicquel *et al.* 2012). The scheme provides third-order space and time accuracy (Colin & Rudgyard 2000). However, because of the explicit nature of the solver, in applications where the viscous sub-layer needs to be computed, mesh refinements force small time steps and a higher computational cost is incurred than for incompressible codes. Note that despite this limitation, the unstructured hybrid approach enables refinement of the mesh in zones of interest by using prisms in the wall region (Boileau *et al.* 2012; Collado *et al.* 2012). Five prism layers are used to accurately capture the viscous sub-layer in this work. The initial thickness of the prisms is $\Delta y/Y = 0.0025$, and the size of the tetrahedral cells in the domain is limited to $0.2Y$. These constraints lead to a mesh size of 2.4 million cells with 89 thousand prisms and 470 thousand nodes.

In addition to a no model run, two sub-grid scale (SGS) models were implemented and tested on the separated flow of interest: the dynamic Smagorinsky model and the σ-model (Baya Toda *et al.* 2010; Nicoud *et al.* 2011). The σ-model was developed to overcome observed deficiencies of the static SGS models without using additional test filters required in dynamic models. The SGS stress for that model has several interesting properties: (1) it vanishes in laminar flows and in regions where the resolved field is two-dimensional (including pure shear and solid rotation cases); (2) it generates no sub-grid scale dissipation when the resolved scales are in pure axisymmetric or isotropic contraction/expansion (the former situation corresponds to the impact region of a laminar round jet impinging on a solid plate, the latter is representative of an acoustic monopole); and (3) it has the appropriate cubic behavior in the vicinity of solid boundaries.

	Spalart & Strelets (2000)	CTR DNS	CTR LES	CTR UDNS	AVBP
N_x	1022	1536	512	240	-
N_y	120	300	140	90	-
N_z	120	128	32	32	-
$N_{total} \times 10^6$	14.7	59.0	2.3	0.7	0.5
% of Spalart	100	401	15.6	4.7	3.2
% of CTR DNS	25	100	3.9	1.2	0.8
Δx^+	20	9.7	26.4	57.0	27.5
Δy^+ at $X = 7Y$	1	0.5	1.0	1.6	2.75
Δz^+	6.7	7.6	27.5	29.6	27.5
$S_{effective}$	0.3	0.21	0.21	0.20	0.3

TABLE 1. Resolution and parameters for all cases run.

3. Results

A total of six simulations were performed: a DNS benchmark case (CTR DNS), a wall-resolved LES with the dynamic Smagorinsky model (CTR LES), a highly under-resolved DNS (CTR UDNS), followed by AVBP simulations with the dynamic Smagorinsky model, σ-model, and no model. Parameters for these simulations are summarized in Table 1. The case of Spalart & Strelets (2000) was initially intended to be the benchmark case. However, that case was run using an incompressible spectral code with imposed vorticity-free boundary conditions at the top boundary. For both approaches used here compressible codes were used and the top boundary conditions of Spalart & Strelets (2000) could not be matched exactly. The CTR approach uses a fringe layer formulation that relaxes the solution to the self-similar zero pressure gradient (ZPG) boundary layer solution, whereas the second, AVBP, uses an aspiration condition that is able to match the mass flow rate of the Spalart & Strelets (2000) simulation. The effective top boundary condition in the CTR approach is compared with the Spalart & Strelets (2000) boundary condition in Figure 2; the nominal deceleration parameter $S_{effective} = 0.21$ is less than for Spalart & Strelets (2000) (see Table 1). In all cases simulations were run until the separation bubble stabilized and turbulent flow was well established downstream of reattachment as illustrated in Figures 3 and 4. Results were then averaged over multiple vortex shedding periods. All results obtained are in good qualitative agreement with their respective DNS benchmarks.

The wall pressure coefficients $C_{p_w} = (P_w - P_\infty)/\frac{1}{2}\rho U_0^2$ shown in Figure 5 for the CTR UDNS and LES cases are both in good agreement with the DNS benchmark with the exception of a slight difference in bubble length. The downward slope in C_p in Figure 5 after $x = 5$ indicates the existence of a slight favorable pressure gradient caused by the inflow top boundary condition in that region as seen in Figure 2. This presents a limitation in the applicability of results to the suction side of airfoils in MAVs and blades in turbo-machinery where favorable pressure gradients are seldom encountered (Jones *et al.* 2010). Although weak, the favorable pressure gradient may also artificially improve agreement of CTR LES and UDNS results with the CTR DNS benchmark as compared with AVBP because of its effect on the reattachment location.

At resolutions on the order of 1% of their respective benchmark DNS, and even without models, all CTR and AVBP simulations predict the separation point seen in DNS benchmarks exactly. This can be observed in the first zero-crossing on the wall skin fric-

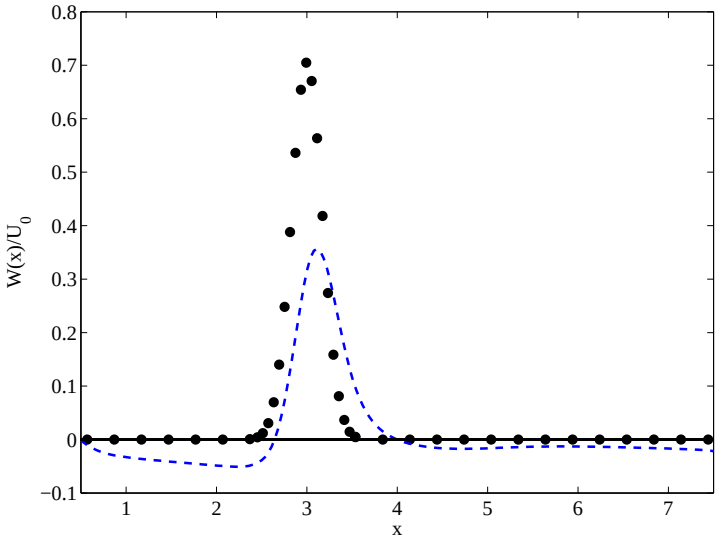

FIGURE 2. Normalized wall-normal velocity top boundary condition. Spalart & Strelets (2000) and AVBP (circles), CTR (dashed line).

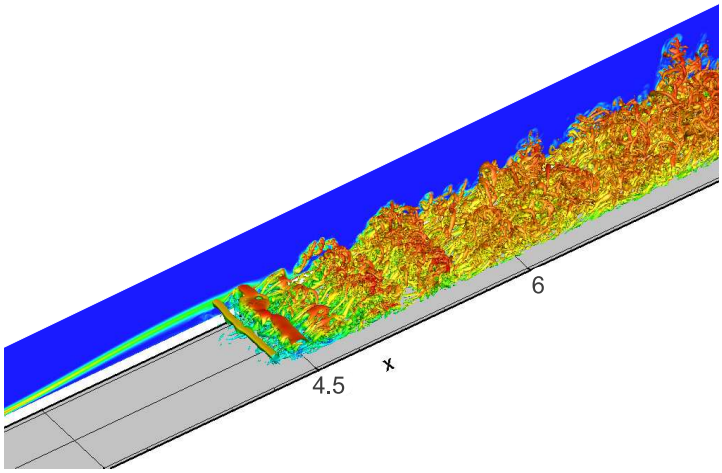

FIGURE 3. Iso-surfaces of vorticity: Kelvin-Helmholtz rolls are visible over the separated shear layer leading to transition to turbulence and subsequent turbulent flow reattachment, closing of the separation bubble.

tion $C_f = (\mu \frac{\partial U}{\partial y}|_{y=0})/\frac{1}{2}\rho U_0^2$ plots in Figures 6 and 7. The peak negative skin friction is consistently under-predicted by nearly 40% in all AVBP simulations, while the CTR UDNS predicts the shape and maximum value of the peak almost exactly. Wall-resolved LES with dynamic Smagorinsky modeling performs slightly worse than the UDNS run, but still reaches within 15% of the DNS peak negative skin friction coefficient value. The length of the bubble is over-predicted in all AVBP runs with a reattachment point approximately 10% farther as indicated by the second C_f zero-crossing in Figure 7. CTR UDNS and LES predict the reattachment point with less than 5% difference with the

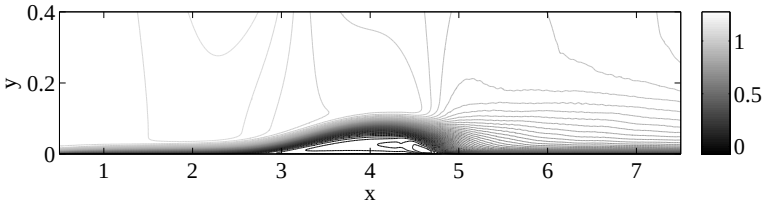

FIGURE 4. Contour plot of normalized average streamwise velocity U/U_0 from the CTR UDNS case. Notice the laminar boundary layer growth followed by a clear separation bubble spanning from $x = 3$ to $x \approx 5$.

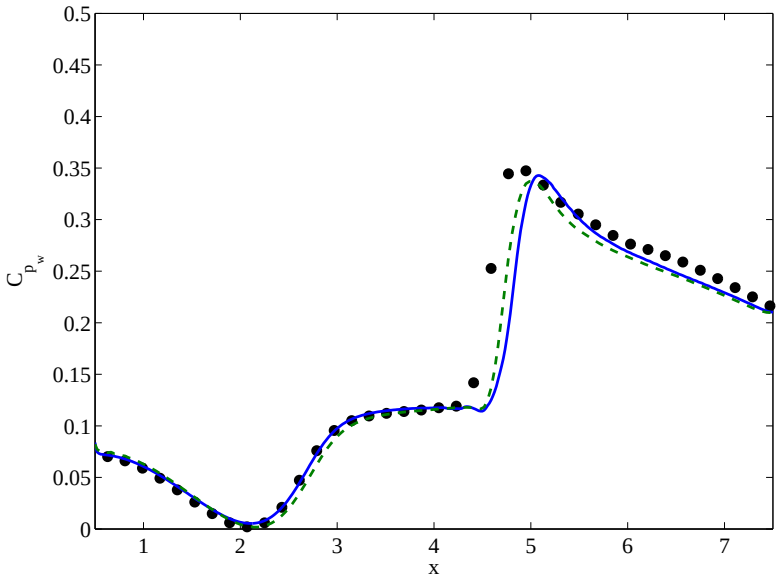

FIGURE 5. Coefficient of pressure at the wall. CTR DNS (circles), CTR LES with dynamic Smagorinsky model (line), CTR UDNS (dashed line).

DNS. CTR UDNS recovers almost exactly the turbulent C_f in the region downstream of the bubble, whereas CTR LES and AVBP results never recover completely.

As is evident in the results presented in Figures 5, 6, and 7, the addition of SGS models visibly worsens agreement with DNS benchmarks. One possible explanation is that the codes used already possess sufficient numerical dissipation through explicit filtering and zonal matching in the case of the CTR code, or truncation error in derivative approximations in the AVBP case. The same cases should be run with non-dissipative codes to assess the accuracy and performance of different SGS models for this particular problem.

4. Conclusions

The capability to predict accurately, at low computational cost, the average skin friction, pressure coefficient and the location of separation and reattachment is of particular interest to airfoil and blade designers. Such capability has been demonstrated for simulations of laminar separation bubble flows at moderate Reynolds number using a resolution on the order of 1% of their fully-resolved DNS counterparts. Satisfactory qualitative

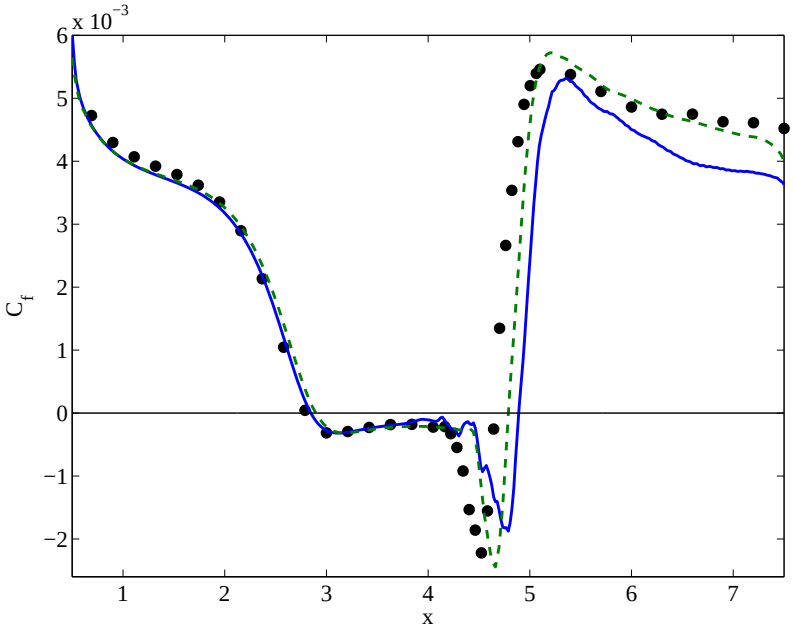

FIGURE 6. Wall coefficient of friction. CTR DNS (circles), CTR LES with dynamic Smagorinsky model (line), CTR UDNS (dashed line).

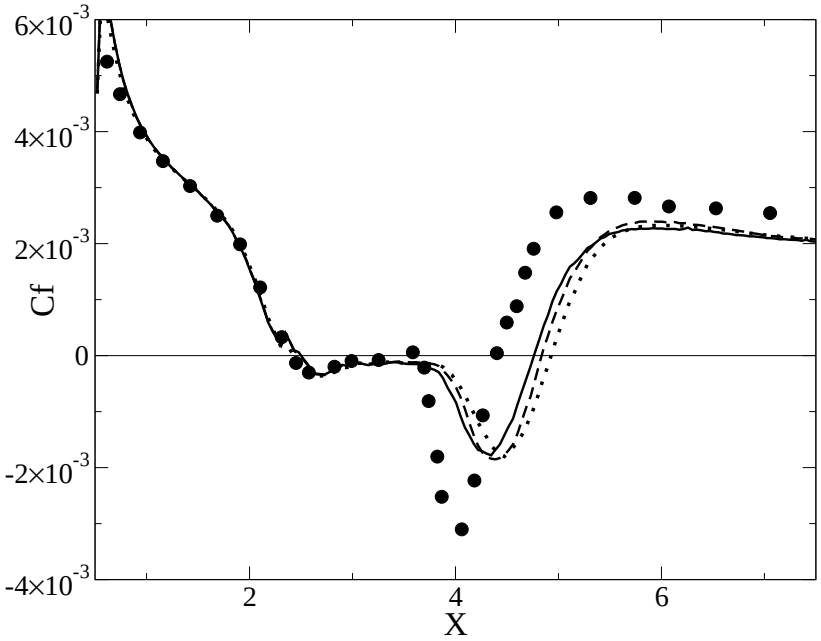

FIGURE 7. Friction coefficient obtained with AVBP. Spalart DNS (circles), no model (line), σ-model (dashed line), dynamic Smagorinsky model (dotted line).

and quantitative agreement was achieved between the highly under-resolved DNS (CTR UDNS), wall-resolved LES with the dynamic Smagorinsky model, and the fully-resolved DNS cases. AVBP results presented good qualitative agreement with Spalart & Strelets (2000) DNS results and predicted separation onset accurately, but consistently under-predicted peak negative skin friction, marginally over-predicted reattachment location, and could not recover the turbulent skin friction coefficient downstream of the bubble.

The relatively good performance of both codes observed in the CTR UDNS and AVBP no-model runs suggests that they may belong to a category of implicit LES where the numerical dissipation plays the role of SGS models. This is reinforced by observing that adding explicit SGS models in both codes consistently worsens agreement with fully-resolved DNS benchmarks. Such behavior is expected for codes that provide enough dissipation through their numerics so that additional explicit SGS dissipation is not required. Both codes used here have obvious sources of numerical dissipation, either explicit filtering or truncation error in derivative approximation. However, without quantifying numerical dissipation effects, the performance and accuracy of different SGS models in dealing with laminar separation bubble flows could not be assessed conclusively. Future work should include quantifying the amount of effective numerical viscosity in the CTR UDNS case, as well as further exploring the effects of SGS models using non-dissipative codes for the same problem.

Acknowledgments

The authors thank Dr. Spalart for providing tabulated aggregate data from Spalart & Strelets (2000) DNS results and for answering questions along the way. The authors also acknowledge the following award for providing computing resources on the CTR Certainty linux cluster toward producing the research results reported within this report: MRI-R2: Acquisition of a Hybrid CPU/GPU and Visualization Cluster for Multidisciplinary Studies in Transport Physics with Uncertainty Quantification (`http://www.nsf.gov/awardsearch/showAward.do?AwardNumber=0960306`). This award is funded under the American Recovery and Reinvestment Act of 2009 (Public Law 111-5).

REFERENCES

Alam, M. & Sandham, N. 2000 Direct numerical simulation of 'short' laminar separation bubbles with turbulent reattachment. *J. Fluid Mech.* **410**, 1–28.

Baya Toda, H., Truffin, K. & Nicoud, F. 2010 Is the dynamic procedure appropriate for all SGS models? In *Fifth European Conference on Computational Fluid Dynamics - ECCOMAS CFD*. Lisbon, Portugal.

Boileau, M., Duchaine, F., Jouhaud, J.-C. & Sommerer, Y. 2012 Large eddy simulation of heat transfer around a square cylinder using unstructured grids. *AIAA J.* **In press**.

Boileau, M., Staffelbach, G., Cuenot, B., Poinsot, T. & Bérat, C. 2008 LES of an ignition sequence in a gas turbine engine. *Combust. Flame* **154** (1-2), 2–22.

Colin, O. & Rudgyard, M. 2000 Development of high-order Taylor-Galerkin schemes for unsteady calculations. *J. Comput. Physics* **162** (2), 338–371.

Collado, E., Gourdain, N., Duchaine, F. & Gicquel, L. 2012 Effects of free-stream turbulence on high pressure turbine blade heat transfer predicted by structured and unstructured LES. *J. Heat Mass Transfer* **55** (21-22), 5754– 5768.

Eisenbach, S. & Friedrich, R. 2008 Large-eddy simulation of flow separation on an

airfoil at a high angle of attack and Re = 10^5 using cartesian grids. *Theor. Comput. Fluid Dynamics* **22**, 213–225, 10.1007/s00162-007-0072-z.

Gicquel, L., Staffelbach, G. & Poinsot, T. 2012 Large eddy simulations of gaseous flames in gas turbine combustion chambers. *Prog. Energy Combust. Sci.* **In press**.

Hain, R., Kähler, C. J. & Radespiel, R. 2009 Dynamics of laminar separation bubbles at low-Reynolds-number aerofoils. *J. Fluid Mech.* **630**, 129–153.

Hu, H., Yang, Z. & Igarashi, H. 2007 Aerodynamic hysteresis of a low-Reynolds-number airfoil. *J. Aircraft* **44** (6), 2083–2085.

Jones, L., Sandberg, R. & Sandham, N. 2010 Stability and receptivity characteristics of a laminar separation bubble on an aerofoil. *J. Fluid Mech.* **648**, 257–296.

Jones, L. E., Sandberg, R. D. & Sandham, N. D. 2008 Direct numerical simulations of forced and unforced separation bubbles on an airfoil at incidence. *J. Fluid Mech.* **602**, 175–207.

Lele, S. K. 1992 Compact finite difference schemes with spectral like resolution. *J. Comput. Physics* **103**, 16–42.

Lin, J. C. M. & L.Pauley, L. 1996 Low-Reynolds-number separation on an airfoil. *AIAA J.* **34** (8), 1570–1577.

Mani, A. 2012 Analysis and optimization of numerical sponge layers as a nonreflective boundary treatment. *J. Comput. Physics* **231** (2), 704 – 716.

Marxen, O., Lang, M. & Wagner, S. 2003 A combined experimental/numerical study of unsteady phenomena in a laminar separation bubble. *Flow, Turbulence and Combustion* **71**, 133–146.

Marxen, O. & Rist, U. 2010 Mean flow deformation in a laminar separation bubble: separation and stability characteristics. *J. Fluid Mech.* **660**, 37–54.

Mendez, S. & Nicoud, F. 2008 Large-eddy simulation of a bi-periodic turbulent flow with effusion. *J. Fluid Mech.* **598**, 27–65.

Nagarajan, S. 2004 Leading edge effects in bypass transition. PhD thesis, Stanford University.

Nagarajan, S., Lele, S. K. & Ferziger, J. H. 2007 Leading-edge effects in bypass transition. *J. Fluid Mech.* **572**, 471–504.

Nicoud, F., H, B. T., Cabrit, O., S., B. & Lee, J. 2011 Using singular values to build a subgrid-scale model for large eddy simulations. *Physics Fluids* **23** (8).

Schønfeld, T. & Rudgyard, M. 1999 Steady and unsteady flows simulations using the hybrid flow solver AVBP. *AIAA J.* **37** (11), 1378–1385.

Spalart, P. & Strelets, M. 2000 Mechanisms of transition and heat transfer in a separation bubble. *J. Fluid Mech.* **403**, 329–349.

Spedding, G. & McArthur, J. 2010 Span efficiencies of wings at low Reynolds numbers. *J. Aircraft* **47** (1), 120–128.

Staffelbach, G., Gicquel, L., Boudier, G. & Poinsot, T. 2009 Large eddy simulation of self-excited azimuthal modes in annular combustors. *Prog. Energy Combust. Sci.* **32**, 2909–2916.

Wilson, P. & Pauley, L. 1998 Two-and three-dimensional large-eddy simulations of a transitional separation bubble. *Physics Fluids* **10**, 2932–2940.

Yang, Z. & Voke, P. 2001 Large-eddy simulation of boundary-layer separation and transition at a change of surface curvature. *J. Fluid Mech.* **439**, 305–333.